Nonlinear Microrheology Reveals Entanglement-Driven Molecular-Level Viscoelasticity of Concentrated DNA

Cole D. Chapman[1] and Rae M. Robertson-Anderson[2,*]
[1]Department of Physics, University of San Diego, San Diego, California 92110, USA
[2]Department of Physics, University of California San Diego, La Jolla, California 92093, USA
(Received 29 April 2014; revised manuscript received 8 July 2014; published 28 August 2014)

We optically drive a trapped microscale probe through entangled DNA at rates up to 100× the disentanglement rate (Wi ≈ 100), then remove the trap and track subsequent probe recoil motion. We identify a unique crossover to the nonlinear regime at Wi ≈ 20. Recoil dynamics display rate-dependent dilation and complex power-law healing of the reptation tube. The force response during strain exhibits key nonlinear features such as shear thinning and yielding with power-law rate dependence. Our results, distinctly nonclassical and in accord with recent theoretical predictions, reveal molecular dynamics governed by individual stress-dependent entanglements rather than chain stretching.

DOI: 10.1103/PhysRevLett.113.098303 PACS numbers: 83.60.Df, 82.35.Pq, 83.80.Rs, 87.85.gf

Microrheology, which uses embedded microspheres as probes, has recently emerged as a powerful technique for characterizing the molecular-level viscoelastic response of a wide range of soft materials and complex fluids, ubiquitous in industry, biology, and daily modern life [1–8]. Microliter sample sizes enable the characterization of valuable and difficult to produce materials, such as DNA and cytoskeleton networks, inaccessible to bulk macrorheology techniques. Physiological scales of induced stresses (piconewtons) and strains (microns) are also directly applicable to a range of biological processes such as cell locomotion, blood flow, and elimination of pathological respiratory mucus comprised of entangled DNA [9], as well as new drug delivery techniques [10].

Linear microrheology measurements, which use passive probe motion or small force probe oscillations, can readily determine microscale linear rheological properties via generalized Stokes-Einstein relations [3], provided the probe is larger than a characteristic length scale of the material [11]. While numerous studies have provided critical insight into the microscale linear viscoelastic properties of entangled polymers and other soft materials [1–8,12–15], far fewer have investigated the nonlinear regime in which the probe is actively driven (via magnetic or optical tweezers) to significantly deform the material from equilibrium [13,16,17]. Here, interpretations within a macrorheology framework are complicated by the inherently inhomogeneous flow fields induced [6,18]. Thus, while microrheology has the unique ability to directly elucidate the molecular-level source of nonlinear material behavior, careful experimental design and interpretation, currently lacking in the literature, are critical.

Further, the reptation tube model, pioneered by de Gennes [19] and Doi and Edwards (DE) [20], remarkable in its ability to predict linear properties of entangled polymers [21], fails to fully capture intriguing nonlinear effects such as shear thinning and yielding, proving ill equipped to explain potential polymer disentanglement at high strain rates [22,23]. According to the tube model, each polymer is confined to move within a tubelike region formed by surrounding entangling polymers, restricting motion transverse to the polymer contour. Tube-model extensions, such as chain stretching and convective constraint release (CCR), have been proposed to accurately explain nonlinear effects [24–30], but conflicting experimental results and theories leave the regime controversial [31,32]. Previously, we used optical tweezers to characterize the near-equilibrium tube potential confining entangled DNA and found evidence of rate-dependent tube dilation not predicted by DE theory and anharmonic tube softening for large strains [15], in accord with recent simulations [33,34]. A recent theoretical model proposed by Sussman and Schweizer (SS) [25,26,30] for entangled rigid polymers predicts an anharmonic potential induced solely by individual topological constraints and coupled to the external stress imposed. Results of the SS model are consistent with previous extensions to DE theory that introduce CCR dynamics [28,29] as well as experimental and simulation results for flexible polymers [33–36]. Conversely, Lu, Wang, and co-workers (LW) [24,36] propose that chain stretching is the dominant mechanism underlying nonlinear features such as a stress overshoot during shear [16,23]. As such, experiments that directly elucidate the underlying molecular dynamics leading to widely observed nonlinear effects are needed [31,32].

Here, we present a novel microrheology technique, using optical tweezers, able to directly characterize the molecular-level viscoelastic response of entangled DNA. We identify a unique crossover to nonlinearity at strain rates ~20 times faster than the disengagement rate (i.e., the rate for a polymer to reptate out of its confining tube). We quantify for the first time the nonlinear spring constant

associated with microscale viscoelasticity, which we show arises primarily from individual DNA entanglements that are coupled directly to induced stress, with chain stretching playing a minimal role. The results resolve a long-standing debate regarding the molecular dynamics underlying the nonlinear response of entangled polymers. Further, our technique and analysis can be used to characterize the microscale nonlinear viscoelastic properties of a wide range of complex fluids and materials.

Double-stranded 45 kbp DNA was prepared, as previously described [37], by replication of a cloned fosmid construct in *E. coli*, followed by extraction, purification, and restriction enzyme treatment to convert supercoiled constructs to linear form. DNA solutions were prepared in an aqueous buffer [10 mM Tris-HCl (pH 8), 1 mM EDTA, 10 mM NaCl] at concentrations of 0.3, 0.5, and 1.0 mg/ml corresponding to $0.5c_e$, c_e, and $2c_e$, respectively, where c_e is the critical entanglement concentration [38]. We can determine corresponding tube diameters d_T and disengagement times τ_d by combining our previous results from linear oscillatory rheology experiments on 45 kbp DNA ($d_T \approx 0.7$ μm at 1 mg/ml, $G_N^0 \sim c^{1.8}$) [11] with tube theory scaling predictions [20]. We estimate $\tau_d \approx 0.72$, 1.24, and 2.57 s and $d_T \approx 1.3$, 1.0, and 0.7 μm for 0.3, 0.5, and 1.0 mg/ml, respectively. Trace amounts of 4.5 μm microspheres (probes) coated with Alexa-Fluor-488 BSA were embedded in DNA solutions which equilibrated for ~30 min prior to measurements.

A custom-built force-measuring optical trap, formed by a 1064 nm Nd:YAG fiber laser focused with a 60 × 1.4 NA objective, was used to trap a probe within the sample chamber. A nanopositioning stage displaced DNA solutions 30 μm relative to the trapped probe at speeds $v = 1$–60 μm/s, which can be expressed as strain rates via $\dot{\gamma} = 3v/\sqrt{2}a$, where a is the probe radius [17]. To compare measured rates to characteristic relaxation rates for each solution, we report all speeds as Weissenberg numbers $\mathrm{Wi} = \dot{\gamma}\tau_d$. Several other groups have used a similar strain ramp technique to probe soft material linear dynamics [5,15,39]. Following strain, the probe remained trapped for wait times t_w of 0–20 s ($0\tau_d$–$27.6\tau_d$), after which the trap was shut off and the subsequent probe position was tracked. An experimental schematic is shown in Fig. 1. All reported data are an average of ≥10 trials. All measurements were repeated in water and viscous unentangled dextran solutions. Both controls exhibited purely Newtonian Stokes flow fluid behavior (Fig. S1 [40]).

A position-sensing detector measured the laser deflection during strain at 20 kHz, while probe images were recorded at 100 s^{-1} both during and after strain. The laser deflection and probe displacement from the trap center during the strain are both proportional to the force acting on the trapped probe over the entire force range accessed. The trap was calibrated via the *in situ* equipartition method in our DNA solutions [5,14] and Stokes drag in water [41].

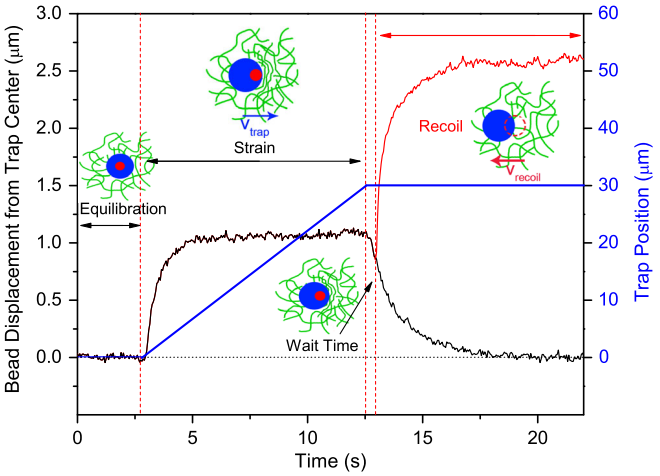

FIG. 1 (color online). Experiment schematic. Trap position (blue line, right axis) and probe displacement from the trap center (black and red curves, left axis) vs time are shown for the four stages of the experiment with cartoons depicting the probe (blue circle), trap center (red dot) and DNA (green). Equilibration: The probe is trapped, and probe and DNA solution equilibrate. Strain: Trap is driven 30 μm at a constant speed v_{trap} through solution. Wait time: Following strain, the trapped probe begins to return to the trap center. Recoil: The trap is shut off, and the probe recoils backward (red curve) with speed v_{recoil}. Black and red curves are an average of 10 trials at 3 μm/s strain speed in 1.0 mg/ml DNA. The black curve during the recoil stage shows a full return of the probe to the trap center if the laser is not shut off.

Measured force curves closely approximate the fluid response, as we find no detectable difference in measured traces when trap stiffness is increased ~2×. For ease of rheological interpretation, the measured force F and trap displacement x are converted to stress and strain via $\sigma = F/\pi a^2$ and $\gamma = x/2a$, respectively.

We find [Fig. 2(a)] that the force exerted on the probe during strain initially increases with displacement (i.e., elastic response) before eventually yielding to a plateau (i.e., viscous response). Such yielding, a key feature of nonlinear strains, arises from unrecoverable microstructure rearrangement due to chain disentanglement and sliding [13,22]. We quantify the strain at which the DNA yields γ_y as the point at which the differential modulus of the force response ($K = d\sigma/d\gamma_{\mathrm{trap}}$), which characterizes the elasticity or stiffness of the material [Fig. 2(b)], drops to $(2e)^{-1}$ of its peak value [Fig. 2(d)]. We find that for $\mathrm{Wi} \leq 10$, γ_y increases linearly with strain speed, indicative of the linear regime in which the relaxation rate is constant (i.e., unperturbed entanglement density). For $\mathrm{Wi} \geq 20$, we find approximate scaling $\gamma_y \sim \mathrm{Wi}^{1/3}$, in agreement with previous macrorheology experiments on entangled melts and suggested to arise from a loss of entanglements or tube softening [24,26,35]. Within this framework, σ_y should be proportional to γ_y, which we find for strains >0.5 [inset of Fig. 2(d)]. While LW suggest that entanglement reduction is due primarily to chain stretching, not accounted for in SS theory [24,36], it also

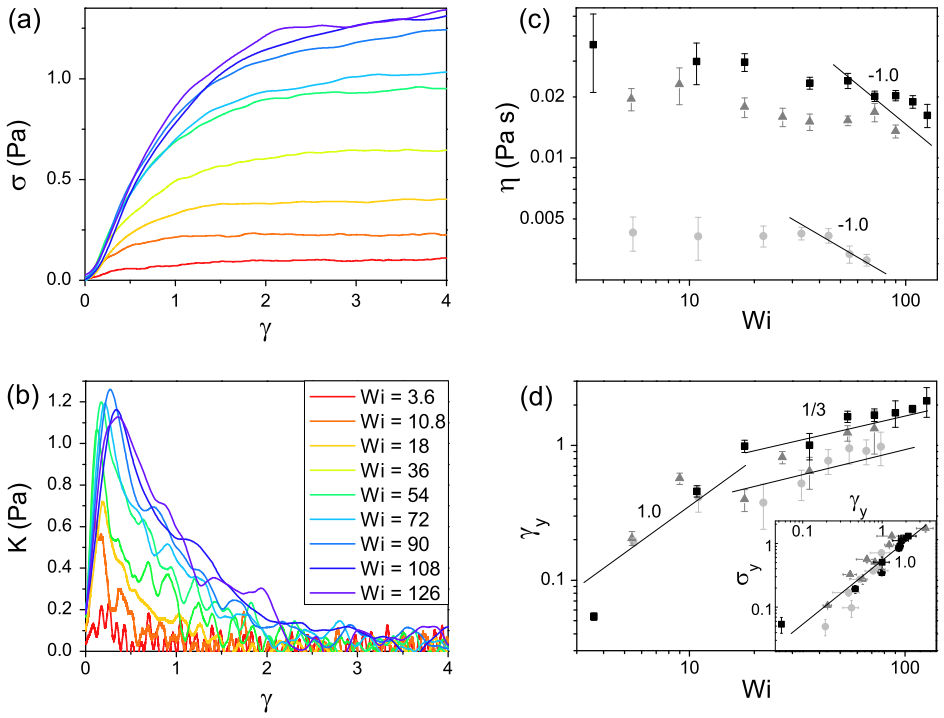

FIG. 2 (color online). DNA response during the constant rate strain. (a) Measured stress σ vs strain γ in 1.0 mg/ml DNA for strain rates Wi = 3.6 to 126 [see the legend in (b)]. (b) Corresponding differential modulus K vs strain for each strain rate. (c) Apparent viscosity η vs strain rate for 0.3 (circles), 0.5 (triangles), and 1.0 mg/ml (squares) DNA with predicted scaling $\eta \sim \mathrm{Wi}^{-1}$ shown. (d) Yield strain γ_y vs Wi for DNA solutions shown in (c) with predicted scaling for linear ($\gamma_y \sim \mathrm{Wi}^{1.0}$) and nonlinear regimes ($\gamma_y \sim \mathrm{Wi}^{1/3}$). The inset shows yield stress σ_y vs γ_y and predicted scaling $\sigma_y \sim \gamma_y$.

shows that significant chain stretch is the source of stress overshoots experimentally seen in macrorheology studies on entangled flexible polymers, including DNA [16,23]. We find no such overshoot, in accord with previous rheology studies on filamentous actin solutions and gelatins as well as SS predictions [13,26,42]. This key difference between our measurements and macrorheology measurements on DNA highlights the unique system dynamics each technique probes [6] and shows that chain stretching only plays a significant role at the level of many-chain dynamics. Further, for very fast rates, the yield strain appears to be asymptoting to a plateau with values of $0.7 > \gamma_y > 2$ in agreement with SS predictions. Note that our results are distinctly nonclassical, as DE predicts a yield stress and strain that are both independent of strain rate with $\gamma_y \sim 2.25$.

From the measured force plateaus (corresponding to $K \approx 0$), we calculate an apparent viscosity via Stokes drag $\eta = F/6\pi a\nu$, which is roughly rate independent for Wi < 20 and then decreases, approaching a scaling of $\eta \sim \mathrm{Wi}^{-1.0}$ [Fig. 2(c)], in accord with macrorheology experiments that show shear-thinning exponents of -0.5 to -1 [20,23]. Classical DE theory predicts shear thinning in the nonlinear regime but with -1.5 scaling, while tube-model extensions that include CCR-like phenomena accurately capture experimental results [26–29].

Following a post-strain wait time t_w, the trap is removed, after which the probe appeared to jump back or "recoil" towards its original position (Figs. 1 and 3). The tracked position of the probe vs time [Fig. 3(a)] fits well to a decaying exponential, from which we determined a maximum recoil distance R and a decay rate β for each strain [Figs. 3(b) and 3(c)]. Our control data showed no measurable recoil, indicating that the recoil is an elastic effect dependent on entanglements. Thus, while the system has yielded to the strain by releasing some entanglements, the tube confinement has not been completely destroyed [25,35]. If the principal hindrance to probe recoil is individual entanglements, then the recoil distance should be comparable to the tube diameter, in line with our results [Fig. 3(b)]. More importantly, we find R increases with Wi, crossing from linear scaling to $R \sim \mathrm{Wi}^{0.4}$ at $\mathrm{Wi} \approx 20$. While the low Wi scaling is indicative of a linear response, the high Wi scaling is in accord with SS predictions for the strain-rate dependence of tube dilation arising from direct coupling of the tube potential to the external stress (rather than simply shear induced affine deformation) [26]. Further, R reaches $\sim 5d_T$, in excellent agreement with the tube radius expansion calculated by previous flexible polymer simulations [33]. The wait-time dependence of R shows $R \leq d_T$ for wait times $t_w > O(\tau_D)$, demonstrating the coupled effect of the tube retracting to its equilibrium size (i.e., lost entanglements reforming) and those entanglements partially relaxing.

This dynamic entanglement reformation and relaxation is more readily seen in the wait-time dependence of the

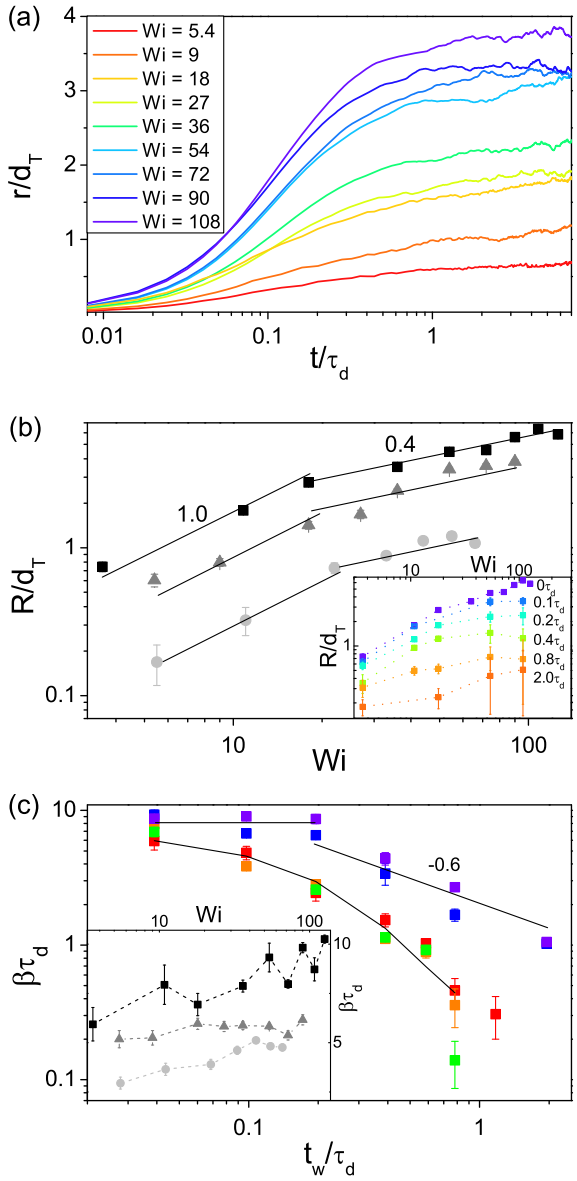

FIG. 3 (color online). Probe recoil dynamics following strain. (a) Measured probe recoil r (normalized by tube diameter d_T) vs time (normalized by disengagement time τ_d) when released immediately after strain (wait time $t_w = 0$). Strain rates of Wi = 5.4 to 108 in 0.5 mg/ml DNA are shown. (b) The maximum recoil distance reached R vs Wi for 0.3 (circles), 0.5 (triangles), and 1.0 mg/ml (squares) DNA at $t_w = 0$ with predicted scaling exponents for linear (1.0) and nonlinear (0.4) regimes. The inset shows R vs Wi for $t_w = 0$ to $2\tau_d$ in 1.0 mg/ml DNA. (c) Measured recoil decay rate β vs t_w for 1.0 mg/ml DNA at Wi = 3.6 (red squares), 10.8 (orange squares), 18 (green squares), 54 (blue squares), and 108 (violet squares) with predicted scaling for linear (exponential curve) and nonlinear (0, −0.6) regimes. The inset shows β vs Wi for $t_w = 0$ for all three DNA solutions.

recoil decay rate β [Fig. 3(c)]. We find that β decreases with t_w but with distinctly different time dependences for Wi above and below ~20. For Wi < 20, the decay is exponential, as expected for a single constant rate relaxation mechanism (i.e., relaxation of the static deformed tube as predicted by DE). For Wi > 20, we find a short-time plateau followed by $\beta \sim t^{-0.6}$ scaling, in agreement with the disengagement time scaling $\tau_D \sim t^{0.6}$ predicted by SS [25]. Further, the two-step power-law relaxation is in close agreement with SS predictions for the stress relaxation following a constant shear strain, explained as an initial fast relaxation mechanism coupled to tube retraction (giving the short-time plateau), followed by simultaneous relaxation of the deformed entanglements (predicted by DE) and tube contraction (slowing the relaxation rate to a power law). We also find that β increases with Wi in line with the strain-rate-dependent relaxation rate predicted by tube theories with CCR-like phenomena [26,29].

To further characterize the microscale stress relaxation, we calculate an effective spring constant associated with entanglements. As the probe recoil fits well to a decaying exponential, we can treat it as that of an overdamped harmonic oscillator and use β to determine an effective entanglement spring constant k via $\beta = [b - (b^2 - 4mk)^{1/2}]/2m$, where $b = 6\pi\eta a$ and m is the probe mass. Calculated spring constants are small enough that $k \sim \beta$, so corresponding rate and time dependences of k are as in Fig. 3(c). Thus, the elastic entanglement stiffness is strain-rate dependent and crosses from linear to nonlinear relaxation dynamics at Wi ~ 20.

For Wi < 20, spring constants are nearly rate independent and increase with concentration, as expected for the linear regime with average values of 3.01, 1.65, and 1.49 pN/μm for the 1.0, 0.5, and 0.3 mg/ml DNA, respectively. We can convert our low Wi spring constant k_L for each concentration to a modulus G_L and compare with the predicted linear modulus $G_e = 3k_bT\rho_e$ [20], where ρ_e is the density of entanglements. Our G_L values are 0.84, 0.46, and 0.41 Pa, in excellent agreement with the predicted values 0.76, 0.43, and 0.29 Pa for 1.0, 0.5, and 0.3 mg/ml DNA. Further, our measured 1.0 mg/ml modulus is in accord with macrorheology plateau modulus measurements for similar DNA solutions (0.65 Pa) [23].

In equilibrium, the elastic energy of each entanglement monomer should be comparable to k_bT. Thus, to confirm that our measured spring constants are indeed due to individual entanglements, we compare our near-equilibrium elastic energy to the thermal energy, i.e., $\frac{1}{2}k_Lx^2 \approx k_bT$. We calculate an approximate equilibrium stretching length scale x, associated with each entanglement of $x \approx 49$, 79, and 88 nm for 1.0, 0.5, and 0.3 mg/ml DNA, respectively. The size of each "entanglement monomer" should be on the order of the mesh size of the solution ζ, which is ~100, 140, and 180 nm for 1.0, 0.5, and 0.3 mg/ml DNA, respectively, giving us $x \approx 0.5\zeta$ and showing that the equilibrium stretching length is comparable to and scales with the entanglement monomer size. Thus, individual DNA entanglements are the source of the microscale elastic response, as confirmed by our other presented

results. If we assume a constant stretching length, as k increases to $\sim 2\times$ the equilibrium value [with increasing Wi; see Fig. 3(c)], the elastic energy exceeds the thermal energy and thus cannot be sustained, so entanglements must be released, reducing the average entanglement density and softening the confining tube.

Here, we have demonstrated a novel experimental technique in which we use an optically trapped probe to drive entangled DNA far from equilibrium and characterize the molecular-level linear and nonlinear viscoelastic responses during and following strain. We show for the first time that microscale nonlinear viscoelasticity for entangled DNA is driven by individual entanglement constraints rather than chain stretching. However, the entanglements are distinctly nonclassical, exhibiting rate-dependent releasing or tube dilation and complex power-law relaxation dynamics. Our results provide critical insights into the long-standing debate on the molecular dynamics underlying the experimentally observed nonlinear response exhibited in entangled polymers. Our technique and analysis can also be used to characterize the microscale viscoelastic properties of a wide range of complex fluids and materials.

This research was funded by the AFOSR Young Investigator Program, Grant No. FA95550-12-1-0315. We would also like to thank Dr. Douglas E. Smith for useful discussions regarding this project.

*randerson@sandiego.edu

[1] T. G. Mason and D. Weitz, Phys. Rev. Lett. **75**, 2770 (1995).
[2] M. Atakhorrami, J. Sulkowska, K. Addas, G. Koenderink, J. Tang, A. Levine, F. MacKintosh, and C. Schmidt Phys. Rev. E **73**, 061501 (2006).
[3] T. M. Squires and T. G. Mason, Annu. Rev. Fluid Mech. **42**, 413 (2010).
[4] J. P. Rich, J. Lammerding, G. H. McKinley, and P. S. Doyle Soft Matter **7**, 9933 (2011).
[5] M. Tassieri, G. M. Gibson, R. M. L. Evans, A. M. Yao, R. Warren, M. J. Padgett, and J. M. Cooper, Phys. Rev. E **81**, 026308 (2010).
[6] T. M. Squires, arXiv:cond-mat/0507551.
[7] M. Gardel, M. Valentine, J. Crocker, A. Bausch, and D. Weitz Phys. Rev. Lett. **91**, 158302 (2003).
[8] D. Chen, E. Weeks, J. Crocker, M. Islam, R. Verma, J. Gruber, A. Levine, T. Lubensky, and A. Yodh Phys. Rev. Lett. **90**, 108301 (2003).
[9] B. K. Rubin, Paediatr. Respir. Rev. **7**, S215 (2006).
[10] J. A. Cribb, T. D. Meehan, S. M. Shah, K. Skinner, and R. Superfine Ann. Biomed. Eng. **38**, 3311 (2010).
[11] C. D. Chapman, K. Lee, D. Henze, D. E. Smith, and R. M. Robertson-Anderson Macromolecules **47**, 1181 (2014).
[12] X. Y. Zhu, B. Kundukad, and J. R. C. van der Maarel, J. Chem. Phys. **129**, 185103 (2008).
[13] J. N. Wilking and T. G. Mason, Phys. Rev. E **77**, 055101(R) (2008).
[14] M. Tassieri, R. M. L Evans, R. L. Warren, N. J. Bailey, and J. M. Cooper New J. Phys. **14**, 115032 (2012).
[15] R. M. Robertson and D. E. Smith, Phys. Rev. Lett. **99**, 126001 (2007).
[16] J. A. Cribb, P. A. Vasquez, P. Moore, S. Norris, S. Shah, M. G. Forest, and R. Superfine J. Rheol. **57**, 1247 (2013).
[17] T. M. Squires, Langmuir **24**, 1147 (2008).
[18] T. M. Squires and J. F. Brady, Phys. Fluids **17**, 073101 (2005).
[19] P.-G. de Gennes, *Scaling Concepts in Polymer Physics* (Cornell University Press, Ithaca, 1979).
[20] M. Doi and S. F. Edwards, *The Theory of Polymer Dynamics*, Oxford Science Publications Vol. 73 (Oxford University Press, New York, 1986).
[21] B. Wang, J. Guan, S. M. Anthony, S. C. Bae, K. S. Schweizer, and S. Granick Phys. Rev. Lett. **104**, 118301 (2010).
[22] S-Q. Wang, Y. Wang, S. Cheng, X. Li, X. Zhu, and H. Sun Macromolecules **46**, 3147 (2013).
[23] R. E. Teixeira, A. K. Dambal, D. H. Richter, E. S. G. Shaqfeh, and S. Chu Macromolecules **40**, 2461 (2007).
[24] S-Q. Wang, S. Ravindranath, Y. Wang, and P. Boukany J. Chem. Phys. **127**, 064903 (2007).
[25] D. M. Sussman and K. S. Schweizer, Macromolecules **45**, 3270 (2012).
[26] D. M. Sussman and K. S. Schweizer, Macromolecules **46**, 5684 (2013).
[27] P. S. Desai and R. G. Larson, J. Rheol. **58**, 255 (2014).
[28] R. S. Graham, A. E. Likhtman, T. C. B. McLeish, and S. T. Milner J. Rheol. **47**, 1171 (2003).
[29] G. Marrucci, J. Non-Newtonian Fluid Mech. **62**, 279 (1996).
[30] D. M. Sussman and K. S. Schweizer, Phys. Rev. Lett. **107**, 078102 (2011).
[31] R. G. Larson, J. Polym. Sci., Part B: Polym. Phys. **45**, 3240 (2007).
[32] A. E. Likhtman, J. Non-Newtonian Fluid Mech. **157**, 158 (2009).
[33] C. Baig, V. G. Mavrantzas, and M. Kröger, Macromolecules **43**, 6886 (2010).
[34] A. Dambal, A. Kushwaha, and E. S. Shaqfeh, Macromolecules **42**, 7168 (2009).
[35] P. E. Boukany, S.-Q. Wang, and X. Wang, J. Rheol. **53**, 617 (2009).
[36] Y. Lu, L. An, S-Q. Wang, and Z-G. Wang ACS Macro Lett. **3**, 569 (2014).
[37] S. Laib, R. M. Robertson, and D. E. Smith, Macromolecules **39**, 4115 (2006).
[38] R. M. Robertson and D. E. Smith, Macromolecules **40**, 3373 (2007).
[39] C. Gutsche, F. Kremer, M. Krüger, M. Rauscher, R. Weeber, and J. Harting J. Chem. Phys. **129**, 084902 (2008).
[40] See Supplemental Material at http://link.aps.org/supplemental/10.1103/PhysRevLett.113.098303 for sample force traces for control data.
[41] P. Wissenburg, T. Odijk, P. Cirkel, and M. Mandel Macromolecules **28**, 2315 (1995).
[42] C. Semmrich, R. J. Larsen, and A. R. Bausch, Soft Matter **4**, 1675 (2008).